A&A 591, A41 (2016)
DOI: 10.1051/0004-6361/201424150

Astronomy & Astrophysics

Broadband observations of the X-ray burster 4U 1705-44 with *Beppo*SAX *(Research Note)*

S. Piraino[1,2], A. Santangelo[2], B. Mück[2], P. Kaaret[3], T. Di Salvo[4], A. D'Aì[1], R. Iaria[4], and E. Egron[5]

[1] INAF–IASF Palermo, via Ugo La Malfa 153, 90146 Palermo, Italy
e-mail: Santina.Piraino@ifc.inaf.it
[2] IAAT University of Tuebingen, Sand 1, 72076 Tuebingen, Germany
[3] Department of Physics and Astronomy, University of Iowa, Iowa City, IA 52242, USA
[4] Dipartimento di Fisica e Chimica, University of Palermo, via Archirafi 36, 90123 Palermo, Italy
[5] INAF–Osservatorio Astronomico di Cagliari, Loc. Poggio dei Pini, Strada 54, 09012 Capoterra (CA), Italy

Received 7 May 2014 / Accepted 6 April 2016

ABSTRACT

Context. 4U 1705-44 is one of the most-studied type I X-ray burster and Atoll sources. This source represents a perfect candidate to test different models proposed to self-consistently track the physical changes occurring between different spectral states because it shows clear spectral state transitions.
Aims. The broadband coverage, the sensitivity and energy resolution of the *Beppo*SAX satellite offers the opportunity to disentangle the components that form the total X-ray spectrum and to study their changes according to the spectral state.
Methods. Using two *Beppo*SAX observations carried out in August and October 2000, respectively, for a total effective exposure time of ∼100 ks, we study the spectral evolution of the source from a soft to hard state. Energy spectra are selected according to the source position in the color-color diagram (CCD).
Results. We succeeded in modeling the spectra of the source using a physical self-consistent scenario for both the island and banana branches (the double Comptonization scenario). The components observed are the soft Comptonization and hard Comptonization, the blackbody, and a reflection component with a broad iron line. When the source moves from the banana state to the island state, the parameters of the two Comptonization components change significantly and the blackbody component becomes too weak to be detected.
Conclusions. We interpret the soft Comptonization component as emission from the hot plasma surrounding the neutron star, hard Comptonization as emission from the disk region, and the blackbody component as emission from the inner accretion disk. The broad feature in the iron line region is compatible with reflection from the inner accretion disk.

Key words. accretion, accretion disks – stars: individual: 4U 1705-44 – stars: neutron – X-rays: stars – X-rays: binaries – X-rays: general

1. Introduction

Hasinger & van der Klis (1989) divided low mass X-ray binaries (LMXBs) in two groups, called Z and atoll sources after the patterns these sources trace out in the X-ray color-color diagram (CCD). The CCD of the Z sources displays a Z-like track, whereas the CCD of atoll sources show a C-like track (Méndez 1999) where two branches can be identified. These are the island and banana states. The island branch is characterized by lower count rates, much less variability in the CCD, and stronger band-limited noise than the banana state.

It has been shown, however, that when sampling the source intensity states of the atoll sources for a long enough time, the shape of their CCD tends to resemble those of Z sources (Gierlínski & Done 2002; Muno et al. 2002). The transient LMXB XTE J1701-462 was the first source to show transitions between all the branches of Z and atoll sources within an outburst lasting a few months (Lin et al. 2009). Also, the transient X-ray pulsar in Terzan 5, IGR J17480-2446, showed atoll and Z-source characteristics during an outburst (Altamirano et al. 2010).

The bright neutron star LMXB 4U 1705-44 was classified by Hasinger & van der Klis 1989, as an atoll source. However, long-term monitoring of this source showed a pattern similar to a complete Z track in the CCD (Gierlínski & Done 2002; Muno et al. 2002; Barret & Olive 2002).

4U 1705-44 is an X-ray burster (Sztajno et al. 1985; Langmeier et al. 1987), whose bursting activity and frequency depends on persistent emission. The source is characterized by variability between low and high intensity states. During the low intensity state, when type I X–ray bursts are most frequent, the spectrum is hard (Langmeier et al. 1987). Barret & Olive (2002), monitoring 4U 1705-44 with the Rossi X-Ray Timing Explorer, observed a spectral state transition soft-hard-soft correlated with the intensity, from a 0.1–200 keV luminosity of 6.9 to 31×10^{36} erg s^{-1}, of a distance to the source of 7.4 kpc (Haberl & Titarchuk 1995). These authors interpreted the observed spectral evolution within a scenario of a truncated accretion disk of varying radius and an inner flow merging smoothly with the neutron star boundary layer (Barret et al. 2000; Done 2002). Barret & Olive (2002) successfully modeled the spectra with a blackbody plus a dominating Comptonized emission (modeled in XSPEC with `compTT`). An iron line whose energy was fixed at 6.4 keV was also detected. The soft component (blackbody) was interpreted as originating from the disk at higher luminosity and from the neutron star surface at lower luminosity.

The Comptonized component was associated with the hot inner flow. Barret & Olive (2002) showed that the truncation radius is not just set by the instantaneous $\dot{M}$, as observations with the same bolometric luminosity have very different spectral and timing properties.

Di Salvo et al. (2005) observed 4U 1705-44 in the energy range 0.3–10 keV with *Chandra*, during a soft state at a luminosity of 33×10^{36} erg s^{-1}, and modeled the spectral continuum with a soft Comptonization model `compTT` (electron temperature $kT_e \sim 2.3$ keV and optical depth $\tau \sim 18$ for a spherical geometry). The iron line K_α at 6.5 keV was found to be intrinsically broad and compatible with a reflection from a cold accretion disk with $R_{in} \sim 15$ km or with a Compton broadening in the external parts of a ∼2 keV corona.

A *XMM-Newton* observation, performed when the source was in a soft state, at $\sim 1.0 \times 10^{38}$ erg s^{-1}, showed that the reflection scenario is the favored solution for explaining the broad emission features (Di Salvo et al. 2009; D'Aì et al. 2010). The broad line of 4U 1705-44, with others lines detected with *XMM-Newton*, is also discussed in Ng et al. (2010) who point out the potential role of the pileup in the broadening of the line. However, recent developments of the subject can be found in Di Salvo et al. (2015), Cackett & Miller (2013), Sanna et al. (2013), Egron et al. (2013), Piraino et al. (2012), Cackett et al. (2012), and Miller et al. (2010).

We report a detailed spectral and timing analysis of two *Beppo*SAX observations of the source performed on August and October 2000. The same data have already been partially used by Fiocchi et al. (2007), Lin et al. (2010), Cackett et al. (2012), and Egron et al. (2013). In fact, our analysis alone uses all *Beppo*SAX NFIs for both observations. Moreover, in our contribution we model the X-ray broadband energy (0.3–200 keV) spectrum of 4U 1705-44 obtained for four different CCD positions (three in the banana state and one in the island state). In particular, we try to fit the both hard and soft spectra with the same model components to highlight the evolution of the spectral parameters along the CCD or hardness intensity diagram. This attempt is similar to the approach of Seifina et al. (2015) based on *Beppo*SAX and RXTE spectra. We also present, for the first time, the *Beppo*SAX Fourier power density spectrum of the source variability in the overall banana and island states. We present the observations, results of the timing, and spectral analysis in Sects. 2–4, respectively, and discuss the results in Sect. 5.

2. Observations

Two *Beppo*SAX observations of 4U 1705-44 were performed August 20–21 2000 (OBS1) and October 3–4 2000 (OBS2), respectively, for a total of 100 ks of on-source observing time.

We obtained spectra from the four *Beppo*SAX Narrow Field Instruments (NFIs) in energy bands selected to provide good signal to noise for this source: the Low Energy Concentrator Spectrometer (LECS; 0.1–4 keV; Parmar et al. 1997), the Medium Energy Concentrator Spectrometer (MECS; 2–10 keV; Boella et al. 1997), the High Pressure Proportional Gas Scintillation Counter (HPGSPC; 4–34 keV; Manzo et al. 1997), and the Phoswich Detection System (PDS; 15–200 keV; Frontera et al. 1997). We extracted the LECS and MECS data in circular regions centered on the source position using radii of 8′ and 4′, respectively, containing 95% of the source flux. We used the same circular regions in the blank field data for background subtraction. As the source is centered along the Galactic bulge, we scaled the blank field background at the source position to the mean level of the background around the source using a factor 2.7 for LECS and 2.64 for MECS. Spectra accumulated from dark Earth data and during off–source intervals were used for background subtraction in the HPGSPC and PDS respectively.

We rebinned the LECS and MECS spectra to sample the instrument resolution with the same number of channels at all energy, and we grouped the HPGSPC and PDS spectra using a logarithmic grid. A normalization factor has been included to account for the mismatch in the *Beppo*SAX instruments absolute flux calibration. The fit values of relative normalization are in good agreement with values typically observed (Fiore et al. 1999).

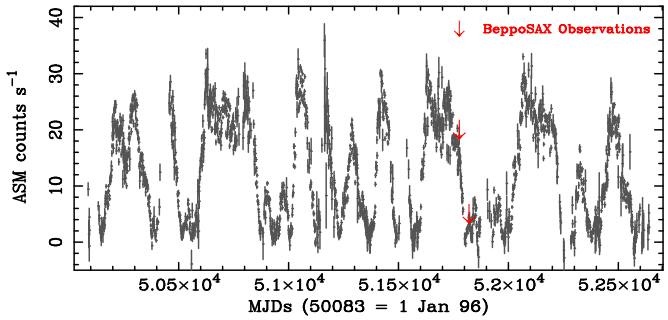

Fig. 1. Long-term (Jan 1996 – Dic 2002) RXTE/ASM 2-12 keV light curve (gray). The data were retrieved from HEASARC public data base. The time of *Beppo*SAX pointed observations (MDJs = 51 766/7 and 51 820/1) are indicated with arrows. During two observation the source intensity changes from ∼300 mCrab to ∼30 mCrab. Overall the source intensity can reach ∼500 mCrab.

3. Timing analysis

Figure 1 shows the RXTE-All Sky Monitor (ASM) light curve (over six years) of 4U 1705-44, where the high long-term X-ray intensity variability is clearly visible. The data of the *Beppo*SAX pointed observations are indicated with arrows. Observation OBS1 (MJDs = 51 766/7) occurred at the beginning of a clear transition from a high to a low intensity state, while during OBS2 (MDJs = 51 820/1) the source was in a low intensity state.

*Beppo*SAX light curves obtained from OBS1 and OBS2 are shown, in different energy range of NFIs, in Fig. 2. A bin size of 1024 s was used. During OBS1 the overall intensity of the source changed up to a factor ∼2 in the range 4.5–30 keV. Six X-ray bursts occurred during the OBS2 observation and were excluded in the subsequent analysis.

Figure 3 shows the power spectral density (PSD) of the OBS1 and OBS2 observations, computed using the MECS data, background (Poisson counting noise level) subtracted, rebinned using a logarithmic scale, and expressed in terms of fractional rms amplitude. In the lower intensity OBS2, the source shows strong band-limited noise and no very low frequency noise, therefore suggesting that the source was in the island state. The observed PSD is typical for these systems characterized by a Lorenzian shape with a break frequency around 0.2 Hz. The PDS for OBS1 is featureless, indicating that the variability during this observation was low.

Figure 4 shows the CCD and the hard color versus intensity diagram (HID) of 4U 1705-44, where the hard color (HC) is the ratio of the 7–10.5 keV to 4.5–7 keV MECS counts rates and the soft color (SC) is the ratio of the 4.5–7 keV to 1–4.5 keV MECS counts rates. The intensity is the count rate in the 1–10.5 keV energy range. Each point corresponds to a time-averaged interval

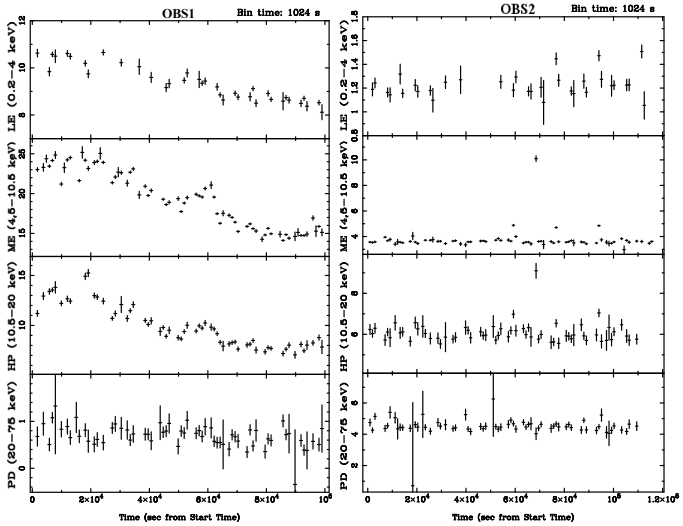

Fig. 2. *Beppo*SAX NFIs light curves during OBS1 (*left*) and OBS2 (*right*). The excess rate in the first tree panels of OBS2 are from X-ray bursts.

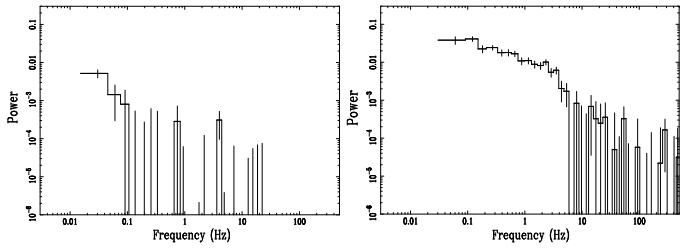

Fig. 3. *Left panel*: PSD in the banana state. *Right panel*: PSD in the island state

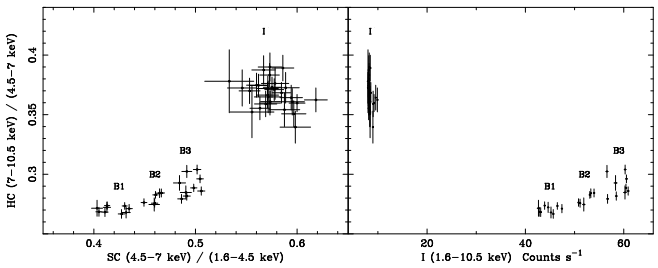

Fig. 4. *Left panel*: color–color diagram. *Right panel*: hardness intensity diagram; the banana and island branches are clearly visible. Energy spectra were extracted in region B1, B2, B3, and I.

of 4096 s. From the CCD and HID diagrams, we conclude that, during OBS1, the source resided in the lower branch of the Z track reported by Gierlinski & Done (2002), Muno et al. (2002), and Barret & Olive (2002). In OBS2, the source is confirmed in the island state, even if the colors are unusual, in that they are very similar to those of the very high part of the banana state. This peculiarity was also observed based on EXOSAT data of 4U 1705-44 (Berger & van der Klis 1998).

In order to investigate the spectral evolution of 4U 1705-44 along the CCD, we extracted the energy spectra of each NFI over four different SC intervals defined by boundaries 0.40–0.44, 0.45–0.47, 0.48–0.51, and 0.53–0.62. We identified three data regions, labeled B1, B2, and B3 in Fig. 4 in the banana state (OBS1), while I is the island state and covers the whole OBS2.

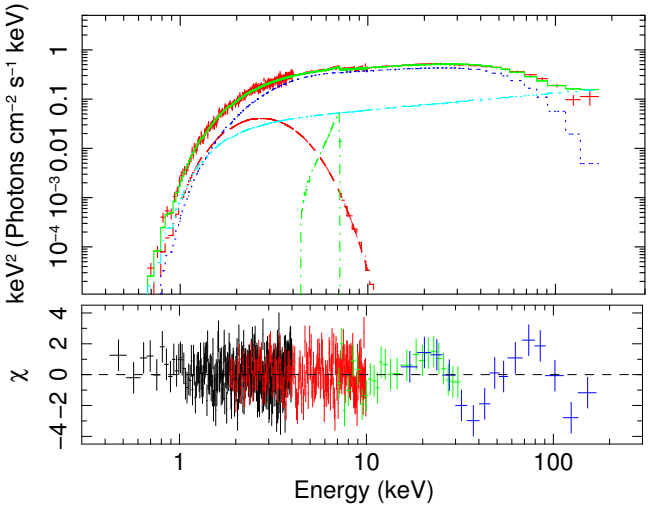

Fig. 5. *Upper panel*: unfolded energy spectrum with Piraino et al. (2007) model and single components in region I. *Bottom panel*: residuals.

4. Spectral analysis

The averaged spectrum of the source for OBS1, that is in the banana branch, was analyzed in Piraino et al. (2007). It is well fitted by a blackbody ($kT_{\rm bb} \simeq 0.56$ keV), contributing ∼14% of the observed 0.1–200 keV flux, plus a Comptonized component modeled with `compTT` (seed photon temperature of ∼1.1 keV, electron temperature ∼2.7 keV, and optical depth ∼11). A hard power-law component (photon index ∼2.9), contributing about 11% of the 0.1–200 keV source flux, was significantly detected. A very broad K_α line at 6.4–6.7 keV (see the above mentioned paper for details) was also reported. The 0.1–200 keV source luminosity is $\sim 10^{38}$ erg s^{-1} assuming a distance to the source of 7.4 kpc (Haberl & Titarchuk 1995).

To investigate the spectral evolution of 4U 1705-44 on the CCD, we fit the broadband spectra extracted from four CCD regions (see Fig. 4) with the model described above. The model adequately fits the data of B1, B2, and B3. However, the spectral continuum of the island state I, fitted with the above mentioned model, shows marked residuals at higher energies (see Fig. 5).

Unfortunately, none the two-component models proposed for the continuum of LMXB, including the western (White et al. 1988), eastern (Mitsuda et al. 1989), Birmingham (Church & Balucinska-Church 1995), or hybrid (Lin et al. 2007), can describe the broadband I spectrum, leaving significant residuals in the highest band. We therefore propose a more complex model to take the origin of this broad residual pattern into account.

To better highlight the structure of the spectrum in Fig. 6, we show the result of a fit with a simple absorbed power-law (the χ^2/d.o.f. was 4801/491). In the residuals we can clearly observe a soft excess, an iron line, and a broad hump over 20–40 keV. That may suggest reflection from a disk. Similar features have been observed in black hole binaries (e.g. Di Salvo et al. 2001; Makishima et al. 2008).

To model the spectrum we firstly used the Poutanen & Svensson (1996) Comptonization model, (`compPS` in XSPEC), which as a built-in function to allow part of the Compton-produced photons to be reflected by cold matter (disk). We thus fitted the I spectrum with the model `wabs*(diskline+compPS)` (Model1), assuming a spherical

Table 1. Best-fit parameters of Model1 and Model2.

	Model1 wabs(compPS+diskline)	**Model2** wabs(bb+compTT+compPS+diskline)			
CDI region	I	I	B1	B2	B3
$N_{\rm H}(\times10^{22}$ cm$^{-2})$	1.18 ± 0.05	1.59 ± 0.03	1.81 ± 0.03	1.76 ± 0.04	1.78 ± 0.04
$kT_{\rm bb}$ (keV)	**	**	0.57 ± 0.03	0.58 ± 0.02	0.58 ± 0.02
$N_{\rm bb} \times 10^{-3}$	**	**	19 ± 2	24 ± 1	24 ± 1
$kT_{\rm W}^{\rm cTT}$ (keV)		0.78 ± 0.02	1.02 ± 0.07	1.15 ± 0.06	1.16 ± 0.06
$kT_{\rm e}^{\rm cTT}$ (keV)		6.7 ± 0.3	2.65 ± 0.08	2.78 ± 0.09	2.71 ± 0.07
$\tau^{\rm cTT}$		7.9 ± 0.3	11.7 ± 0.6	10.4 ± 0.7	11.3 ± 0.7
$N_c^{\rm cTT}(\times10^{-2})$		1.7 ± 0.1	30 ± 3	34 ± 2	42 ± 3
$kT_{\rm e}$ (keV)	27 ± 1	21.6 ± 0.2	31 ± 5	35^{+5}_{-12}	32^{+7}_{-4}
kT_i (keV)	0.74 ± 0.02	0.11 ± 0.08	0.48 ± 0.04	0.47 ± 0.04	0.52 ± 0.02
$\tau^{\rm cPS}$	2.8 ± 0.1	2.94 ± 0.03	0.7 ± 0.1	0.6 ± 0.2	$0.6^{+0.4}_{-0.3}$
$Rel_{\rm refl}$	0.24 ± 0.04	0.27 ± 0.05	2.4 ± 1	3.0 ± 2	4 ± 2
ξ (erg cm s^{-1})	393^{+124}_{-167}	1470 ± 600	3800^{+1500}_{-700}	2600^{+1300}_{-1000}	2800^{+1500}_{-1000}
$N_c^{\rm cPS}(\times10^3)$	201 ± 20	30.7 ± 5	$1.0^{+0.5}_{-0.2}$	$0.7^{+0.9}_{-0.3}$	$0.5^{+0.3}_{-0.2}$
$R_{\rm i}^{\rm cPS}$ (km)	11 ± 1				
$E_{\rm Fe}^{\rm diskline}$ (keV)	6.44 ± 0.09	6.47 ± 0.08	6.43 ± 0.07	6.48 ± 0.08	6.42 ± 0.05
$R_{\rm in}$ (M)	9^{+6}	12^{+5}	7^{+5}	13^{+14}	9.5^{+4}
Incl (deg)	40. fix	40. fix	40. fix	40. fix	40. fix
$I_{\rm Fe}$ ($\times10^{-3}$ ph cm^{-2} s^{-1})	0.9 ± 0.4	1.1 ± 0.2	4.2 ± 0.5	4.2 ± 0.8	6.7 ± 0.9
$\chi^2_{\rm red}$ (d.o.f.)	1.03 (485)	1.05 (482)	1.03 (542)	0.97(544)	1.08(412)

Notes. Model1 consists of a Comptonization component (compPS) and a reflection with emission line (diskline). Model2 consists of a blackbody model (bb) and a double Comptonization component (compTT and compPS with reflection) and the emission line. The two asterisks indicate that the bb component is not required in the I state. When it is added to the model with $kT_{\rm bb}$ fixed to 0.1 keV the value of $N_{\rm bb}$ is $(6 \pm 7) \times 10^{-3}$; the values of the other parameters remain almost unchanged. Uncertainties are at the 90% confidence level for a single parameter.

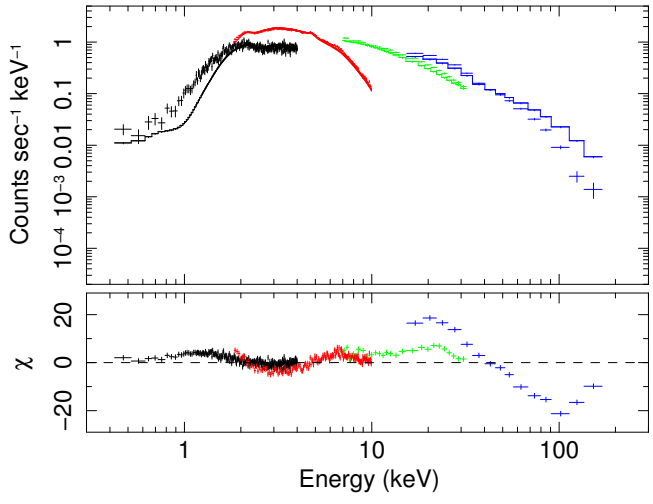

Fig. 6. *Upper panel*: folded spectra and absorbed power-law model. *Bottom panel*: residuals.

geometry for the Compton cloud. We activated the reflection option, assuming a solar abundance for the cold disk matter. We can successfully model the whole (0.3–200 keV) spectrum ($\chi^2/\nu = 1.03$, $\nu = 484$), obtaining a subtended solid angle of $\Omega/2\pi \sim 0.3$ (see first column in Table 1).

Unfortunately, Model1 cannot be applied to the B1, B2, or B3 spectra because in the banana state the electron cloud temperature is ~3 keV (Piraino et al. 2007; Di Salvo et al. 2009; Egron et al. 2013), while the compPS component was considered for electron cloud temperatures $T_{\rm e} > 10$ keV. We also tried to fit the island state spectrum I using the alternative model wabs*(diskline+compTT+compPS) (Model2), containing a soft Comptonization component (compTT) with spherical geometry, plus a second hard Comptonization component (compPS) with disk geometry. In Model2 the soft (*secondary*) Comptonization is thought to originate in the inner region close to the neutron star, where kT_i and $kT_{\rm e}$ is equal to 0.8 and 6.7 keV and $\tau \sim 8$, while the hard (*main*) Comptonization compPS comes from a higher temperature region above the disk, which is characterized by $kT_{\rm e} = 22$ keV, $kT_i = 0.11$ keV and $\tau = 2.9$. The reflection component subtends an angle of $\Omega/2\pi \sim 0.3$ (see second column in Table 1).

Adding a blackbody component bb to Model2, to take the direct emission from the disk into account, we obtain a kT_{bb} value of about 0.1 keV, which is very close to that found for the input photon of compPS. The contribution of this component to the total flux is about 10% of the total flux. However, since the addition of a bb is not statistically significant for Model2, no final conclusion can be obtained about the flux of the direct blackbody emission originating from the disk.

Using Model2 on the average spectrum of the banana states, we obtain a statistically good fit. In this spectrum, the bb component comes out to be statistically significant and the compPS component well describes the hard excess reported in Piraino et al. (2007). However, as shown in the last three columns

Table 2. Best-fit parameters of Model3 and Model4.

	Model3 wabs(bb+compTT+compPS+diskline)				**Model4** wabs(compTB+compTB+diskline)			
CDI region	I	B1	B2	B3	I	B1	B2	B3
$N_{\rm H}(\times10^{22}$ cm$^{-2})$	1.66 ± 0.04	1.67 ± 0.04	1.67 ± 0.04	1.68 ± 0.04	1.59 ± 0.04	1.54 ± 0.05	1.55 ± 0.06	1.56 ± 0.05
$kT_{\rm bb}$ (keV)	$0.1 fix$	0.56 ± 0.03	0.58 ± 0.03	0.58 ± 0.03				
$N_{\rm bb} \times 10^{-3}$	10 ± 10	20 ± 3	22 ± 3	23 ± 3				
$\alpha_{\rm c1}$					0.90 ± 0.02	1.4 ± 0.1	1.7 ± 0.2	1.4 ± 0.2
$kT^{\rm i}_{\rm c1}$ (keV)	0.78 ± 0.02	1.05 ± 0.07	1.14 ± 0.06	1.16 ± 0.06	0.77 ± 0.02	0.99 ± 0.07	1.13 ± 0.06	1.13 ± 0.07
$kT^{\rm e}_{\rm c1}$ (keV)	6.9 ± 0.3	2.7 ± 0.1	2.7 ± 0.1	2.7 ± 0.1	8.6 ± 0.2	3.0 ± 0.2	3.1 ± 0.3	2.9 ± 0.2
$\tau_{\rm c1}$	7.8 ± 0.3	11.1 ± 0.8	10.9 ± 0.8	11.4 ± 0.8				
$N_{\rm c1} \times 10^{-2}$	1.6 ± 0.1	30 ± 4	36 ± 4	43 ± 4	6.7 ± 0.5	42 ± 1	53 ± 1	62 ± 2
$\alpha_{\rm c2}$					0.6 ± 0.1	0. fix	0. fix	0. fix
$kT^{\rm i}_{\rm c2}$ (keV)	0.1 ± 0.001	0.48 ± 0.01	0.48 ± 0.01	0.47 ± 0.01	0.13 ± 0.1	0.52 ± 0.02	0.54 ± 0.02	0.54 ± 0.02
$kT^{\rm e}_{\rm c2}$ (keV)	21.1 ± 0.2	32 ± 1	21 ± 0.7	20^{+1}	19 ± 2	12^{+5}_{-3}	11^{+7}_{-4}	8^{+5}_{-3}
$\tau_{\rm c2}$	2.96 ± 0.01	0.9 ± 0.03	1.46 ± 0.04	1.49 ± 0.04				
$N_{\rm c_2} \times 10^{3}$	33.4 ± 0.8	0.75 ± 0.02	0.77 ± 0.03	0.88 ± 0.03				
$N_{\rm c_2} \times 10^{-3}$					1.8 ± 0.2	18^{+1}_{-2}	20 ± 1	20 ± 1
$E^{\rm diskline}_{\rm Fe}$ (keV)	6.49 ± 0.08	6.46 ± 0.08	6.5 ± 0.1	6.45 ± 0.09	6.48 ± 0.05	$6.5+0.1_{-0.2}$	6.5 ± 0.1	6.45 ± 0.05
$R_{\rm in}$ (M)	9^{+5}	6^{+7}	6^{+9}	10^{+6}	9^{+5}	6^{+10}	14^{+11}	10^{+4}
$I_{\rm Fe}$ ($\times10^{-3}$ ph cm^{-2} s^{-1})	1.4 ± 0.2	4.7 ± 0.8	5.7 ± 0.9	7 ± 1	1.3 ± 0.2	4.8 ± 0.2	4.9 ± 0.7	7.5 ± 1.0
$\chi^2_{\rm red}$ (d.o.f.)	1.09 (481)	1.05 (544)	0.98 (546)	1.07 (414)	1.08 (481)	1.05 (546)	0.98 (548)	1.07 (416)

Notes. Model3 consists of a blackbody model and a double Comptonization component (compTT and compPS without reflection) and an emission line. Model4 consist of two compTB components and the emission line. Uncertainties are at the 90% confidence level for a single parameter.

of Table 1, the Model2 used in the three banana states provides values of the best-fit parameters for the reflection fraction, $\Omega/2\pi > 1$. As a reflection fraction of 1 corresponds an isotropic source above the disk plane, such high values suggest that the model Model2 is not an adequate physical model for this state.

Since our aim is to model the two states with the same model components, we tested double Comptonization models with nonreflection to highlight the evolution of the parameters. The first, Model3, is obtained by turning off the reflection in the compPS component of Model2 and the second, Model4 consists in a double compTB model. The best-fit parameters of the two models are reported in Table 2. Following Titarchuk et al. (2014) in the framework of the applied model wabs*(compTB1+compTB2+diskline) the free parameters of the model are $\alpha_{1/2}$, $kT^{\rm i}_{\rm c1/2}$, $\log(A_{1/2})$, related to the Comptonized fractions $f_{1/2}$, and $kT^{\rm e}_{\rm c1/2}$, $N_{\rm C1/2}$, which are the normalizations of the bb components of the compTB1 und compTB2. We fixed certain parameters of the compTB models, $\gamma_{1/2} = 3$ (related to the index of the low energy part of the spectrum, namely $\alpha_{1/2} = \gamma_{1/2} - 1 = 2$) and $\delta_{1/2} = 0$, because we neglect the bulk inflow effect versus the thermal Comptonization for neutron star accretion. The bulk inflow Comptonization takes place very close to neutron star surface. However, if the radiation pressure in that vicinity is sufficiently high then the bulk motion is suppressed. On the other hand, if mass accretion is low then the effect of the bulk motion is negligible. We also fixed the value of the compTB1 parameter $\log(A_1)$ to 8 when the best-fit values of $\log(A_1) \gg 1$ because in any case of $\log(A_1) \gg 1$ a Comptonization fraction $f = A/(1 + A)$ approaches unity and further variations of $A \gg 1$ do not improve fit quality any more (Titarchuk et al. 2014). Finally, as the values of the parameters α_2 in the banana spectra B1, B2, and B3 are very small, we fixed them to 0. We did not introduce an extra bb component in Model4, which is required in the banana spectra, because it is modeled inside the compTB2 component. In Figs. 7 and 8 we show best-fit components and residuals of the Model4 applied on I and the averaged B spectra, respectively. Using Model3 and Model4, we investigated the spectral behavior versus the position on the CC diagram using the 0.1–100 keV flux to identify the four regions. As shown in Fig. 9, the parameters of the two Comptonization components vary significantly with the position along the CC track. We also studied the relation between the spectral index α_1 of the first compTB and its normalization $N_{\rm c1}$. This is shown in Fig. 10.

5. Discussion

5.1. The island state

The Comptonization model of Poutanen & Svensson (1996), which takes into account that a fraction of Compton-produced photons can be reflected by cold matter (disk), successfully described the spectrum of the island state, that is when a spherical

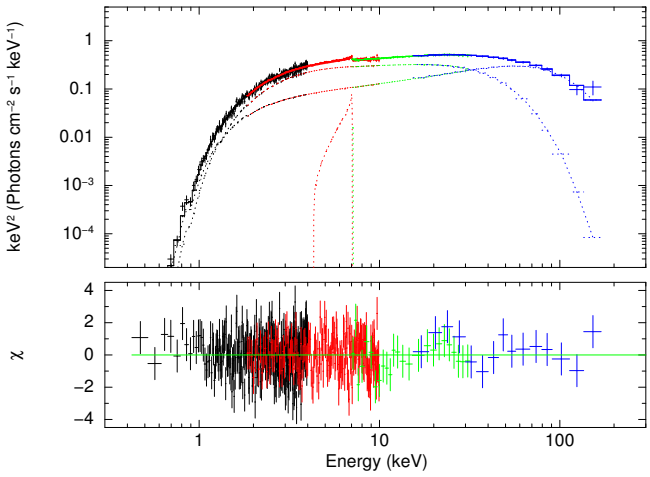

Fig. 7. *Upper panel*: unfolded energy spectrum with model Model4 and single components in region I. *Bottom panel*: residuals

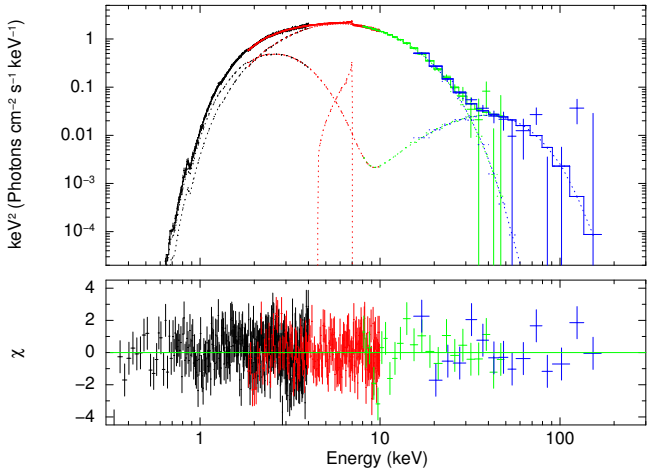

Fig. 8. *Upper panel*: unfolded averaged energy spectrum with model Model4 and single components in region B. *Bottom panel*: residuals.

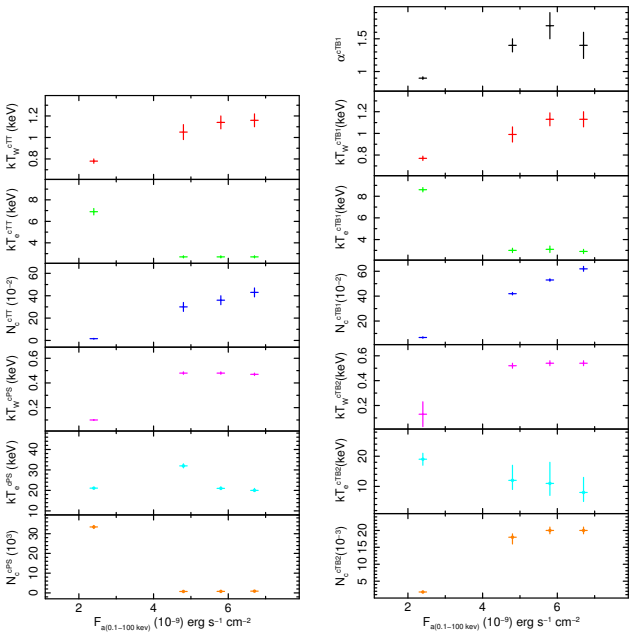

Fig. 9. Best-fit parameters of the Comptonization components vs. the absorbed flux in the range 0.1–100 keV obtained using two different double Comptonization model. *Left panel*: values for Model3. *Right panel*: values for Model4.

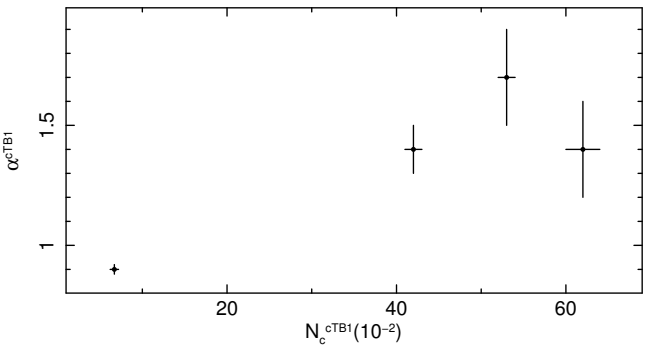

Fig. 10. Spectral index alpha versus normalization of the first `CompTB` component.

geometry of the Compton cloud is assumed together with reflection from a cold disk with solar abundances. More specifically, the model suggests that photons of temperature of $kT_i \simeq 0.7$ keV are Comptonized in a region of electron temperature $kT_e \sim 27$ keV, which is characterized by $R_i = 11$ km. This scenario is naturally interpreted in the context of a truncated accretion disk scenario with the seed input photons coming from the region between the neutron star surface and inner part of the truncated accretion disk, or the boundary layer. The addition of a blackbody component to this model was not statistically significant, suggesting that we did not observe the seed photon component. Recently, Egron et al. (2013), combining data from *XMM-Newton*, RXTE, and *Beppo*SAX (with the exclusion of the PDS instrument), obtained a similar spectral deconvolution using the model `phabs*(nthComp+highecut*rdblur*reflionx)`, which contains a thermally Comptonized continuum (`nthComp`; Zdziarski et al. 1996; Zycki et al. 1999) plus a self-consistent reflection model including both the reflection continuum and the corresponding discrete features (Ross & Fabian 2005). The relativistically smeared `rdblur` kernel (Fabian et al. 1989) was also used. The best-fit parameters that we obtained using the model above are consistent with those reported by Egron et al. (2013). We therefore confirm that during the hard state (observed in October 2000), a viable scenario is given by an absorbed Comptonized component with evidence of reflection from a colder accretion disk (Fabian et al. 1989). The presence of a broad iron emission line at about 6.4 keV and a Compton hump in the 20–40 keV energy range is expected from the reprocessing of the main Comptonization continuum on the accretion disk. However, to find a scenario that could be used in both the island and the banana state, we explored an alternative description of the broadband energy spectrum of the low/hard state of the source: a dual Comptonization of photons in two distinct emission regions. We used `compTT` plus `compPS`, or two `compTB`. The dominant emission results, by the Comptonization, in a disk geometry of seed photons at ~0.1 keV by a plasma with $kT_e \sim 20$ keV and optical depth ~3. This emission can be interpreted as arising in a region above the accretion disk and contributes to the 70% of the total flux. We call this component hard Comptonization. In addition, a secondary emission component, described by a spherical geometry, is due to seed photons at ~0.8 keV Comptonized by a plasma with $kT_e \sim 7$ keV and optical depth ~8 using a `compTT` model or with $kT_e \sim 9$ keV using a `compTB`. This emission can be interpreted as originating from a region closer to the neutron star around the boundary layer and

contributes about 30% of the total flux. We call this component soft Comptonization. The persistent emission spectrum of the LMXB GS 1826-23, observed jointly by *Chandra* and RXTE, has been described by Thompson et al. (2005) with a similar model. This model uses dual Comptonization of ~0.3 keV soft photons by a plasma with $kT_e \sim 20$ keV and $\tau \sim 2.6$, which is interpreted as emission from accretion disk corona, plus Comptonization of hotter 0.8 keV photons by a ~6.8 keV plasma, which is interpreted as emission from the boundary layer. The parameters are therefore very similar to those reported here for 4U 1705-44. Moreover, a dual Comptonization model was successfully applied to the broadband spectra of the low/hard state of the black hole candidate Cyg X-1 by Makishima et al. (2008) with Suzaku data, by Di Salvo et al. (2001) and Frontera et al. (2001) with *Beppo*SAX data, and by Gierliski et al. (2007) and Ibragimov et al. (2005), who used simultaneous Ginga, RXTE and GRO/OSSE data. Takahashi et al. (2008) modeled the spectra of GRO J1655–40 taken with Suzaku in a similar way. Recently, the two `compTB` model was applied to six neutron star LMXBs (see Seifina et al. 2015). This model describes a scenario in which the Keplerian disk is connected to the neutron star by the transition layer (see Titarchuk et al. 1998), where the hot electrons scatter off the soft photons from the neutron star photosphere of temperature kT_1 and the soft disk photons of temperature kT_2 giving rise to two Comptonized components. We stress that no reflection component is needed in the two scenarios described above.

5.2. Banana states and high energy tail

The absorbed Comptonized component with reflection does not describe the soft/high state spectrum. In addition to a dominating Comptonized emission, the continuum broadband spectrum of the source during the soft state requires a blackbody component at lower energies and a hard component to model the hard tail or excess. The dual Comptonization scenario successfully describes the broadband spectra of the banana state in that it models the soft dominating emission and the hard tail well. Contrary to the island state, the dominating Comptonization emission is soft and is expected to originate in the hot plasma surrounding the neutron star. The parameters of this component change significantly when the source moves in the banana branch and with respect to the island state. Its contribution to the flux changes from 57% to 66% for the three banana states.

The hard Comptonization shapes the hard excess emission originating from the disk region and its contribution to the flux is ~17% of the 0.1–200 keV source flux and changes with the CCD position. With respect to the island state flux, the flux of the soft Comptonization is increased by 400%. The flux of the hard Comptonization is reduced by 25%. The low energy emission is modeled by a blackbody that we interpret as originating from the accretion disk. The blackbody component contributes ~22% of the observed 0.1–200 keV flux and changes with the position in the CCD.

We note that a different scenario was analyzed in Piraino et al. (2007). In that case, we described the average banana branch spectrum by the sum of a blackbody, a Comptonized component, and a hard energy tail. The hard energy tail, described with a steep power-law with photon index ~2–3 without evidence of a high energy cutoff, could be produced, as proposed for Z-sources, either in a hybrid thermal/nonthermal model (Poutanen & Coppi 1998) or in a bulk motion of matter close to the neutron star (e.g. Titarchuk & Zannias 1998). The alternative mechanism proposed is the Comptonization of seed photons by high-velocity electron of a jet (e.g. Di Salvo et al. 2000) or the synchrotron emission from a relativistic jet escaping the system (Markoff et al. 2001). We refer to Piraino et al. (2007) for details on this scenario and on similarities with black holes.

6. Conclusions

In this Note, we have presented a spectral-timing analysis of the full set of the *Beppo*SAX observations of 4U 1705-44. In our analysis, for the first time ever, all available data from the *Beppo*SAX NFIs were used. As a result of our analysis, we obtained 1) the broadband X–ray spectra of the source, from soft to hard X-rays (0.3–200 keV) for different spectral states, that is for the island and banana branches; 2) the PSDs in the island and banana branches and the CCD diagram for all available observations; and 3) broadband spectra resolved with respect to the position of the source in the CCD diagram.

Using these results, we confirmed through the PSD that the source was, indeed, in hard state during OBS2 and we succeeded in modeling the spectra of the source using the same physical scenario for both the island and banana branches (the double Comptonization scenario).

According to this scenario, the following components are observed: 1) soft Comptonization arising from the hot plasma surrounding the neutron star and dominant during the banana state; 2) hard Comptonization from the disk region and dominant during the island state; 3) blackbody component arising from the inner part of the accretion disk and not observed in the island state; and 4) broad features in the K_α iron line region observed in both banana and island states, which are modeled well with the `diskline` model.

The evidence of a possible reflection component in the broadband energy spectrum of the island state favors the interpretation of the iron line as a emission from the accretion disk. However, in the double Comptonization scenario no reflection is required. We cannot therefore exclude that broad lines can originate in the outflow from the disk.

Finally, we wish to stress that the double Comptonization model appears as the more suitable solution to describe the spectral behavior of the source during all different states observed with *Beppo*SAX.

Acknowledgements. This work was supported by INAF and IAAT. The High-Energy Astrophysics Group of Palermo acknowledges support by the Fondo Finalizzato alla Ricerca (FFR) 2012/13, project N. 2012-ATE-0390, founded by the University of Palermo, by the Region of Sardinia through POR-FSE Sardegna 2007-2013, L.R. 7/2007, Progetti di Ricerca di Base e Orientata, Project N. CRP-60529, and by the INAF/PRIN 2012-6. E. Egron acknowledges financial support from the Autonomous Region of Sardinia through a research grant under the program CRP-25399 PO Sardegna FSE 2007-2013, L.R. 7/2007, promoting scientific research and innovation technology in Sardinia. We thank the anonymous referee for her/his comments and Amy Mednick for language editing.

References

Altamirano, D., Homan, J., Linares, M., et al. 2010, ATel, 2952, 1
Barret, D., & Olive, J. F. 2002, ApJ, 576, 391
Barret, D., Olive, J. F., Boirin, L., et al. 2000, ApJ, 533, 329
Berger, M., & van der Klis, M. 1998, A&A, 340, 143
Boella, G., Chiappetti, L., Conti, G., et al. 1997, A&AS, 122, 327
Cackett, E. M., & Miller, J. 2013, ApJ, 777, 47
Cackett, E. M., Miller, J., Reis, R. J., et al. 2012, ApJ, 755, 27
Church, M. J., & Balucinska-Church, M. 1995, A&A, 300, 441
D'Aì, A., Di Salvo, T., Ballantyne, D., et al. 2010, A&A, 516, A36
Di Salvo, T., Stella, L., Robba, N. R., et al. 2000, ApJ, 544, 119
Di Salvo, T., Done, C., Zychi, P. T., et al. 2001, ApJ, 547, 1024

Di Salvo, T., D'Aì, A., Iaria, R., et al. 2009, MNRAS, 398, 2022
Di Salvo, T., Iaria, R., Matranga, M., et al. 2015, MNRAS, 449, 2794
Done, C. 2002, Philos. Trans. R. Soc. London A., 360, 1967
Egron, E., Di Salvo, T., Motta, S., et al. 2013, A&A, 550, A5
Fabian, A. C., Rees, M. J., Stella, L., & White, N. E. 1989, MNRAS, 238, 729
Fiocchi, M., Bazzano, A., Ubertini, P., et al. 2007, ApJ, 657, 448
Fiore, F., Guainazzi, M., & Grandi, P. 1999, Cookbook for BeppoSAX NFI Spectral Analysis
Frontera, F., Costa, E., Dal Fiume, D., et al. 1997, A&AS, 122, 357
Frontera, F., Zdziarski, A. A., Amati, L., et al. 2001, ApJ, 561, 1006
Gierlínski, M., & Done, C. 2002, MNRAS, 331, L47
Haberl, F., & Titarchuk, L. 1995, A&A, 299, 414
Hasinger, G., & van der Klis, M. 1989, A&A, 225, 79
Ibragimov, A., Poutanen, J., Gilfanov, M., et al. 2005, MNRAS, 362, 1435
Langmeier, A., Sztajno, M., Hasinger, G., Truemper, J., & Gottwald, M. 1987, ApJ, 323, 288
Lin, D., Remillard, R. A., Homan, J. 2007, ApJ, 667, 1073
Lin, D., Remillard, R. A., & Homan, J. 2010, ApJ, 719, 1350
Makishima, K., Takahashi, H., Yamada, S., et al. 2008, PASJ, 60, 585
Manzo, G., Giarrusso, S., Santangelo, A., et al. 1997, A&AS, 122, 341
Markoff, S., Falcke, H., & Fender, R. 2001, A&A, 372, L25
Miller, J. M., D'Aì, A., Bautz, M. W., et al. 2010, ApJ, 724, 1441
Mitsuda, K., Inoue, H., Nakamura, N., & Tanaka, Y. 1989, PASJ, 41, 97M
Muno, M. P., Remillard, R., & Chakrabarti, D. 2002, ApJ, 568, L35
Ng, C., Diaz Trigo, M., Cadolle Bel, M., & Migliari, S. 2010, A&A, 522, A96
Parmar, A. N., Martin, D. D. E., Bavdaz, M., et al. 1997, A&AS, 122, 309
Piraino, S., Santangelo, A., Di Salvo, T., et al. 2007, A&A, 471, L17
Piraino, S., Santangelo, A., Kaaret, P., et al. 2012, A&A, 542, L27
Poutanen, J., & Svensson, R. 1996, ApJ, 470, 249
Poutanen, J., & Coppi, P. S. 1998, Phys. Scr., T77, 57
Ross, R. R., & Fabian, A. C. 2005, MNRAS, 358, 211
Sanna, A., Hiemstra, B., Méndez, M., et al. 2013, MNRAS, 432, 1144
Seifina, E., Titarchuk, L., Shrader, C., & Shaposhnikov, N. 2015, ApJ, 808, 142
Sztajno, M., Langmeir, A., Frank, J., et al. 1985, IAU Circ No. 4111
Takahashi, H., Fukazawa, Y., Mizuno, T., et al. 2008, PASJ, 60, 69
Titarchuk, L., & Zannias, T. 1998, ApJ, 493, 863
Titarchuk, L., Seifina, E., & Shrader, C. 2014, ApJ, 798, 98
Thompson, T. W. J., Rothschild, R. E., Tomsick, J. A., & Marshall, H. L. 2005, ApJ, 634, 1261
White, N. E., Stella, L., & Parmar, A. N. 1988, ApJ, 324, 363
Zdziarski, A. A., Johnson, W. N., & Magdziarz, P. 1996, MNRAS, 283, 193
Zycki, P. T., Done, C., & Smith, D. A. 1999, MNRAS, 309, 561